

Corrosion Behavior of Ferrite-Pearlite Steel Exposed to H₂S/CO₂ Environment

Hongyan Wang^{1,*}, Chi Yu^{1,2}, Xiuhua Gao^{1,*}, Linxiu Du¹, Hongwei Wang²

¹ The State Key Laboratory of Rolling and Automation, Northeastern University, Shenyang 110819, China;

² School of Resource and Material, Northeastern University at Qinhuangdao, Qinhuangdao 061000, China

*E-mail: hongyanwang0309@163.com, gaoxiuhua@126.com

Received: 21 January 2020 / Accepted: 3 April 2020 / Published: 10 June 2020

The corrosion characteristics of ferrite-pearlite steel under H₂S-CO₂-Cl⁻ environment are studied by accelerated corrosion test and electrochemical experiment. The micromorphologies and crystal structures of corrosion products are analyzed by scanning electron microscopy (SEM) and X-ray diffraction (XRD), the mass loss and potentiodynamic polarization techniques are studied on corrosion rate of the test steel. The results show that H₂S dominates the whole corrosion process and seriously affects the corrosion properties, it changes the corrosion products significant differences on structure with immersion time, ultimately stable corrosion products pyrrhotite can effectively reduce corrosion rate, and provide good protection to the steel matrix.

Keywords: ferrite-pearlite steel, corrosion behavior, H₂S-CO₂-Cl⁻ environment, mass loss, potentiodynamic polarization

1. INTRODUCTION

The corrosion problem of alloy steel is an increasing concern in the oil and gas field, it will bring great destruction [1-4]. H₂S is highly soluble in water triggering the release of hydrogen ions, it can capture electrons and the simultaneous accelerate electrowinning of iron at the anodic [5-7]. The corrosion properties of material under H₂S-CO₂-Cl⁻ environment are very complex due to interaction between the physical and chemical characteristics. At present, the mostly widely used in industry is ferrite-pearlite steel since it is more cost-effective. Therefore, it is very crucial to deeply understand the corrosion mechanism.

Recently, H₂S/CO₂ corrosion has attracted more attention, some results have been proposed to research the effect various environments on corrosion resistance, such as temperature, pH value, alloy element, microstructure, and so on [8-25]. But the papers on the long period corrosion are seldom

reported probably because of the highly toxic of H_2S . It is known that the corrosion products play an important role, and exist various crystal structures under $H_2S-CO_2-Cl^-$ environment, the detailed mechanism is not yet understood completely. In view of the above analysis, the work is motivated to study the corrosion behavior of ferrite-pearlite steel with immersion time.

The corrosion resistance of ferrite-pearlite steel after long period immersion under H_2S/CO_2 environment is investigated in this paper. The corrosion properties are systematically studied in term of microstructure, surface morphology, corrosion phases, cross sectional morphology, corrosion rate and potentiodynamic polarization curve. It is better to study the corrosion mechanism of ferrite-pearlite steel, which will provide great value for oil and gas field.

2. EXPERIMENTAL PROCEDURE

2.1 Materials

The chemical composition of ferrite-pearlite steel (wt.%) is: C 0.14, Si 0.3, Mn 1.15, P 0.016, S 0.008, Al 0.028, Cu 0.06, Nb 0.02, Ti 0.015, Cr 0.0015 and Fe balance. The raw materials are smelted and forged. The samples are obtained by thermo-mechanical control process with the stages of metal rolling including rolling temperature for $848^\circ C$, final cooling temperature for $661^\circ C$ and cooling rate for $10.1^\circ C/s$. The samples are machined into a size of $25\text{ mm} \times 60\text{ mm} \times 5\text{ mm}$, and ground up to 800 grit abrasive SiC paper. The distilled water and ethanol are used to dust and grease, and dried by nitrogen. The specimens are weighted by balance with very high precision.

2.2 Immersion tests

Immersion tests are performed in autoclave with 5 L capacity to provide a high temperature and high pressure environment, the schematic diagram of test equipment is shown in Fig.1.

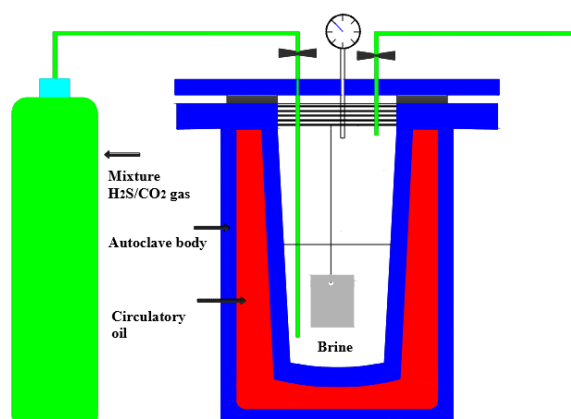


Figure 1. Schematic diagram of autoclave setup for the corrosion test

The tested electrolyte is 3.5 wt% NaCl solution. First, the test specimens are placed in the autoclave, and then sealed. The temperature is controlled at 75°C by circulatory oil system. Second, N₂ gas is pumped into the corrosion medium for 2 h. Third, the H₂S/CO₂ is injected into the electrolyte until the pressure is 1.2 MPa (0.09 MPa H₂S, 0.64 MPa CO₂ and 0.47 MPa N₂). After corrosion experiment, the samples are rinsed with deionized water and alcohol, dried thoroughly by nitrogen. The corrosion scale is removed by the chemical cleaning method using the ASTM G1-03 standard [26]. The corrosion rate is given according to the following equation.

$$v = \frac{8.76 \times 10^4 \times (W_1 - W_2)}{S \times T \times \rho} \quad (1)$$

where v is the corrosion rate (mm/year), W_1 and W_2 are the start and end weight of sample (g), respectively, S is the surface area (cm²), T is the immersion time (h), ρ is the density of sample (7.85 g/cm³).

2.3 Electrochemical measurements

All test samples server as the work electrodes, which are cut to 10mm×10mm×3mm and embedded in epoxy with the area of exposed is 10mm×10mm. Before the test, it is indispensable that the working surface is polished with SiC waterproof abrasive papers of 1500 grits. The electrochemical experiments are conducted with PATSTAT2273 workstation.

The test solutions are in use by 3.5 wt.% NaCl, it is necessary that the open circuit potential is stabilized and ready for 50 min prior to each electrochemical test. All the potentiodynamic polarization curves are measured with the potential scan rate 0.5mV/s. Each electrochemical experiment is completed thrice to maintain high accuracy of experimental results, and analyze the potentiodynamic polarization curves with the CorrWiew software.

3. RESULTS AND DISCUSSION

3.1 Microstructure

The microstructures of experimental steel are presented in Fig.2, the pearlite (P) and ferrite (F) microstructures are observed by the SEM. The TEM figures show that the gray white area is ferrite matrix, and the black strip is cementite. Meanwhile, the average grain size of ferrite and pearlite are 12.1 microns and 11.1 microns, respectively, the content of pearlite is 23.1% using metallographic analysis software.

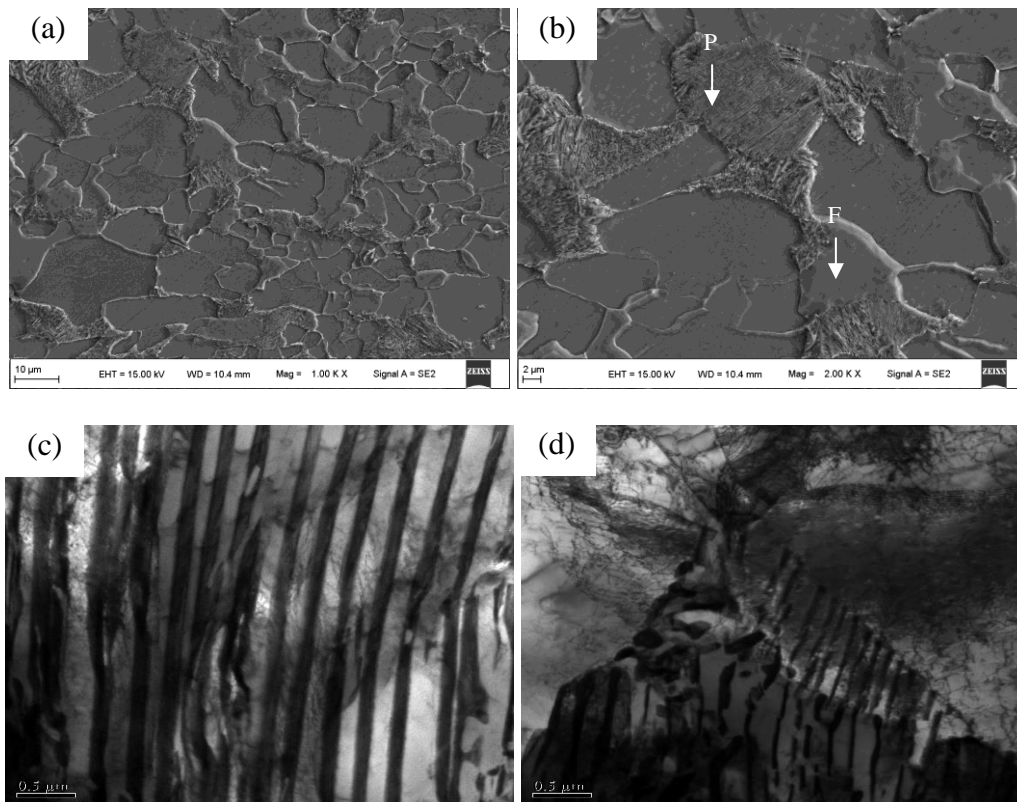


Figure 2. Microstructure properties of experimental steel showed by (a) and (b) SEM; (c) and (d) TEM

3.2 Corrosion surface morphology

The morphologies obtained from different immersion time of ferrite-pearlite steel under H_2S/CO_2 environment are shown in Fig.3, and typical EDX results are given in Fig.4. The results manifest that the atomic ratio of Fe/S between 1.02 and 1.41 as mackinawite of tetragonal, troilite with hexagonal is about 1, and pyrrhotite with monoclinic or hexagonal is between 0.79 and 0.95 [27].

The mackinawite of corrosion products are found in the entire corrosion process. Fig.4a indicates that the mackinawite includes 52.03 % of iron atom and 47.97% of sulfur atom, Fe/S atomic ratio is 1.08, it is iron-rich FeS corrosion product. The ferrite-pearlite steel is soaked for 24 hours, the corrosion particles are larger, and the arrangement between particles is looser. The corrosion products do not cover the steel matrix completely, and there are corrosion cracks at the local position, which can result in pitting corrosion due to the immersion of corrosion particles, the behavior will be detrimental to corrosion resistance. As the corrosion scales thickens, it will break and fall off due to the stress caused by the volume effect [28]. When the steel is immersed for 48 hours, it is seen that the large particles may fall off or dissolve, forming fine corrosion products on the surface of the sample. After being corroded for 96 hours, the corrosion products become more fine and compact, it will improve the corrosion rate. It is found that Mackinawite formed by solid-state reactions is semi-stable form of iron sulfide, other forms of iron sulfide are formed mainly by precipitation, which show the mackinawite forms much faster than any other iron sulfide [29].

When the experimental steel reaches the later stage of corrosion, the parts of mackinawite converts into the new corrosion products with troilite and pyrrhotite. Troilite is the intermediate corrosion product, as shown in Fig.4b, it contains 50.43 % of iron atom and 49.57% of sulfur atom, Fe/S atomic ratio is about 1. The pyrrhotite is characterized by a hexagonal prism-like crystal, and the elongated hexagonal crystals appear to be formed from the trigonal precursor.

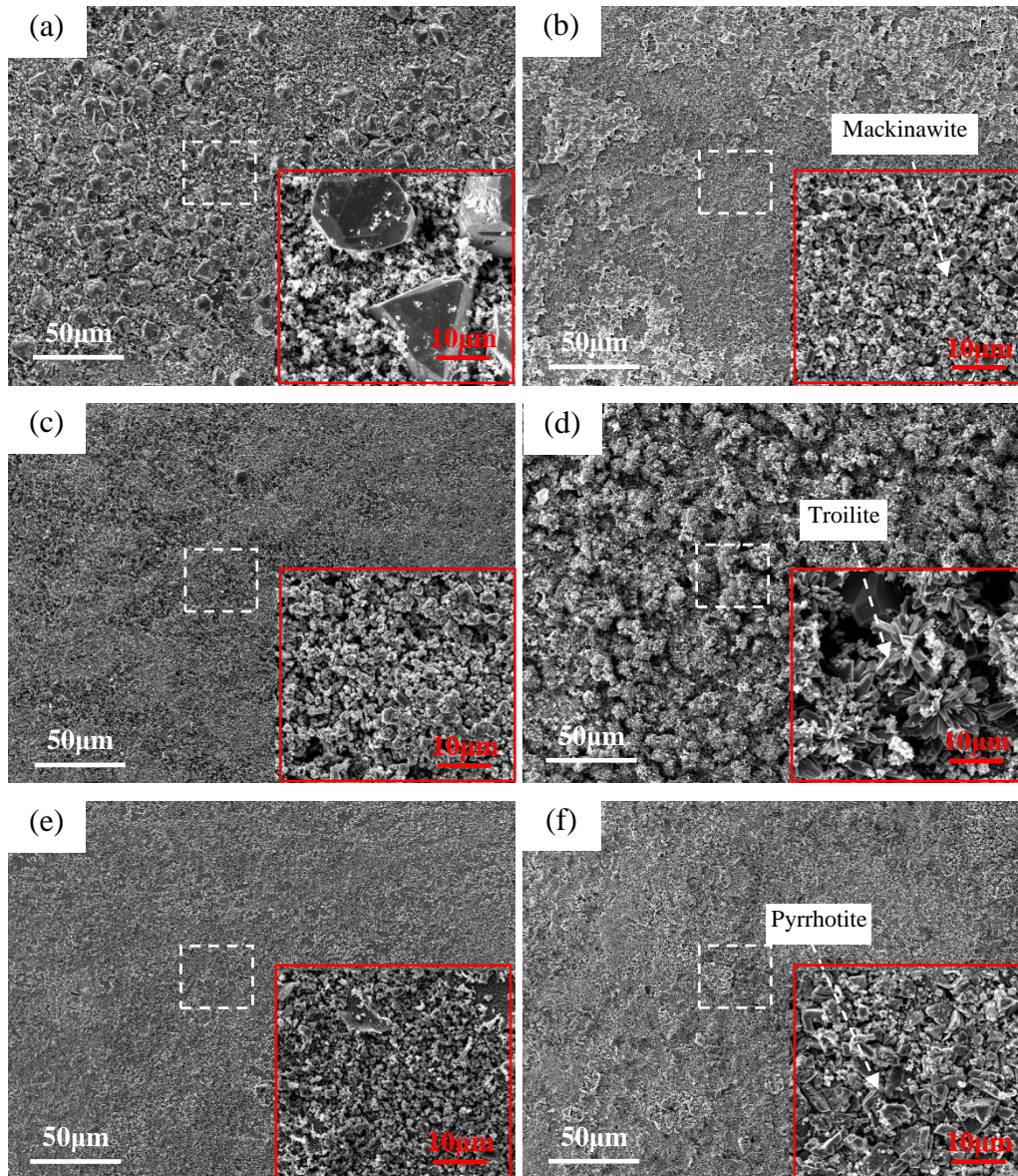


Figure 3. Surface corrosion morphology of ferrite-pearlite steel under H_2S/CO_2 environment at $75^\circ C$ after different immersion time: (a)24 h (b)48 h (c)96 h (d)192 h (e)288 h (f)384 h. The illustration shows the enlarged form of the marked position with white dashed line.

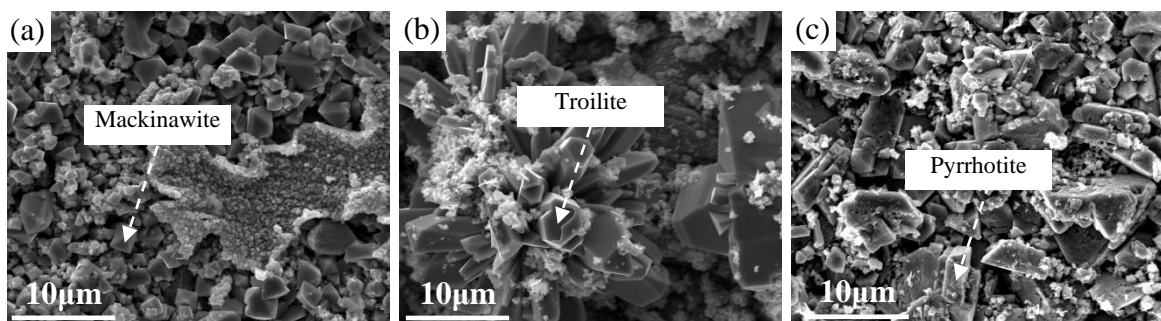
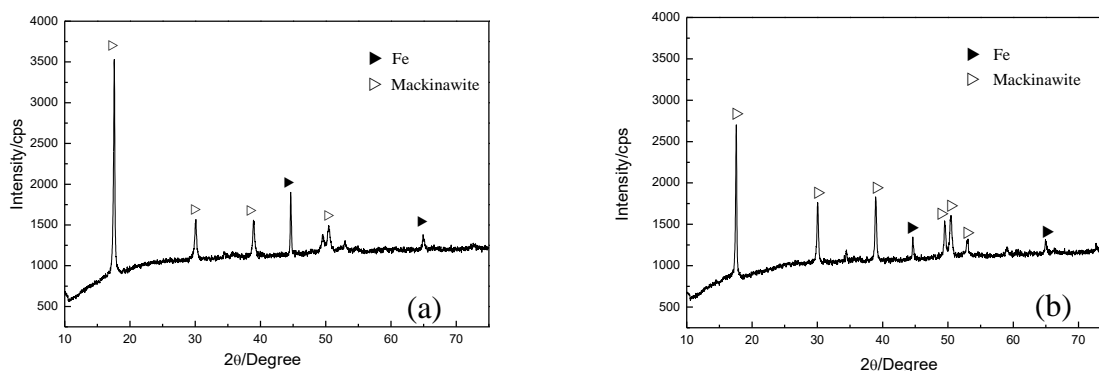


Figure 4. EDX results of ferrite-pearlite steel under H_2S/CO_2 environment at $75^\circ C$ after different immersion time: (a)48 h (b)192 h (c)384 h

Fig.4c shows that the pyrrhotite contains 46.78 % of iron atom and 53.22% of sulfur atom, Fe/S atomic ratio is 0.88, it is a sulfur-rich corrosion product. The concentration of sulfide ion increases with immersion time, and form sulfur-richer pyrrhotite. Meanwhile, the particles become more uniform and dense.

3.3 Corrosion phases

Fig.5 provides XRD patterns of ferrite-pearlite steel exposed to the H_2S/CO_2 environment. According to the test data and theoretical analysis, the types of different corrosion products are observed. The corrosion products contain different types of iron sulfide, which indicates that H_2S corrosion has an important role [30-31]. Fe is found when test steel is immersed for 24 and 48 hours, and the thin corrosion films and a few corrosion products are found. When the immersion time reaches 96 hours, Fe is not detected, it indicates that the surface of samples is completely covered by corrosion products. The corrosion products grow and adhere, the mackinawite and troilite are observed, and the number of characteristic peaks and height of mackinawite are more than these of troilite, the troilite is minor corrosion phases. The pyrrhotite is main corrosion product during the later corrosion period. The analysis results are consistent with the corrosion morphology as described above.



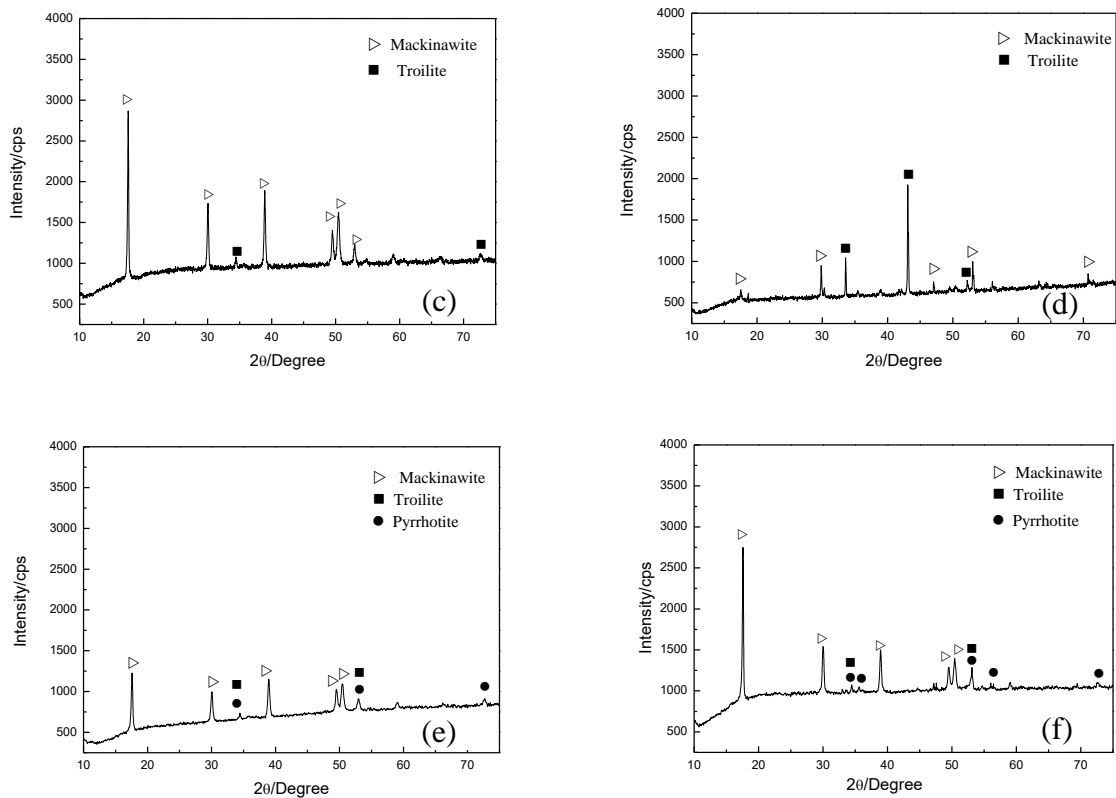


Figure 5. XRD pattern of ferrite-pearlite steel under H_2S/CO_2 environment at $75^\circ C$ after different immersion time: (a)24 h (b)48 h (c)96 h (d)192 h (e)288 h (f)384 h

3.4 Cross section morphology

The cross section morphologies of ferrite-pearlite steel are shown in Fig.6. The corrosion scales have two-layer structures. As shown in Fig.6 (a), we can see that a thin inner layer about $0.6-1.0 \mu m$ and a sparse outer layer ranges from $7 \mu m$ to $15 \mu m$, the particles of corrosion products are relatively large, and the steel substrate is seriously damaged. When the test steel is immersed for 48 hours, the inner layer is destroyed, a discontinuous inner layer is observed. When immersion time reaches 96 hours, the thickness of inner layer becomes thicker (about $27 \mu m$) and more compact. The thickness of corrosion product scales increases with immersion time, the steel substrate is covered about $37 \mu m$ Fe-S compounds after 384 hours, the inner layer is more compact and denser, the corrosion resistance is improved, this is due to a uniform layer of corrosion product cover the surface.

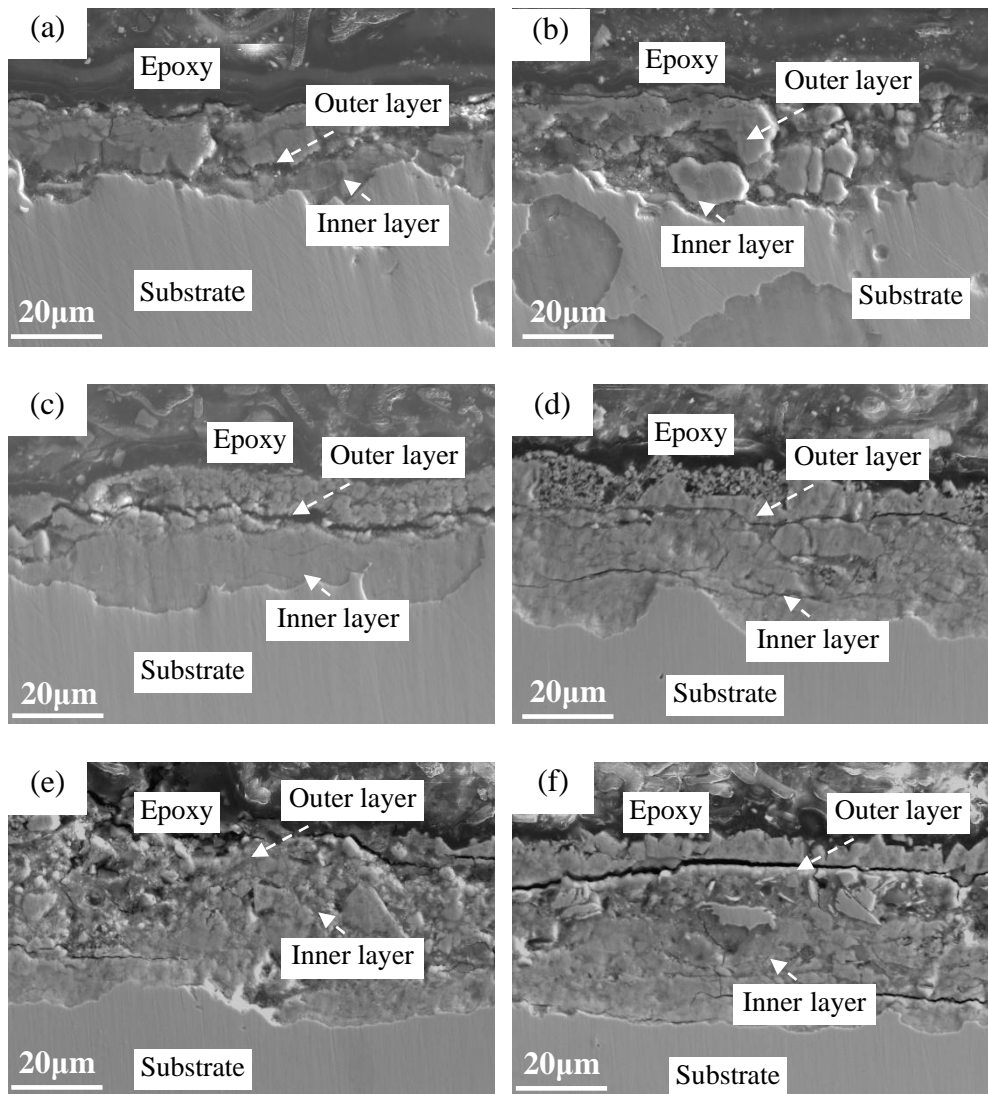


Figure 6. Cross-section morphology of ferrite-pearlite steel under H_2S/CO_2 environment at $75^\circ C$ after different immersion time: (a)24 h (b)48 h (c)96 h (d)192 h (e)288 h (f)384 h

3.5 Corrosion kinetics

Fig.7 shows the corrosion rate of ferrite-pearlite steel with immersion time. It shows three distinguishable stages. In the early stages, it goes down very quickly, and changes slowly, finally the corrosion rate is almost constant after immersion 192 hours. It is related to the structural characteristics of corrosion products and thickness of corrosion product film. The results (Fig.3 and Fig.6) show the corrosion products are compact and the films are uniform when the steels are immersed after 92 hours, so the corrosion rates become small, which show our analysis is correct.

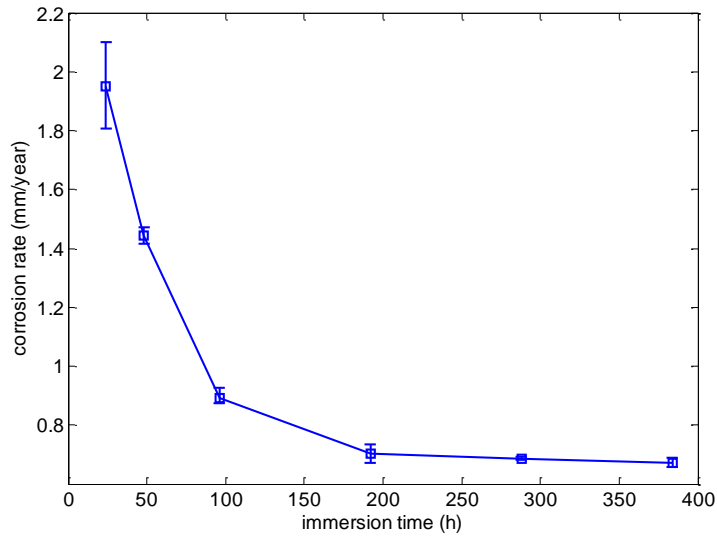


Figure 7. The corrosion rate of ferrite-pearlite steel under H₂S/CO₂ environment at 75°C after different immersion time

3.6 Potentiodynamic polarization curve analysis

The electrochemical corrosion behavior is studied by the potentiodynamic polarization curve measurement to analyze the samples after different immersion time. Fig.8 describes as the typical polarization curves of studied samples after 24, 48, 96, 192, 288 and 384 hours.

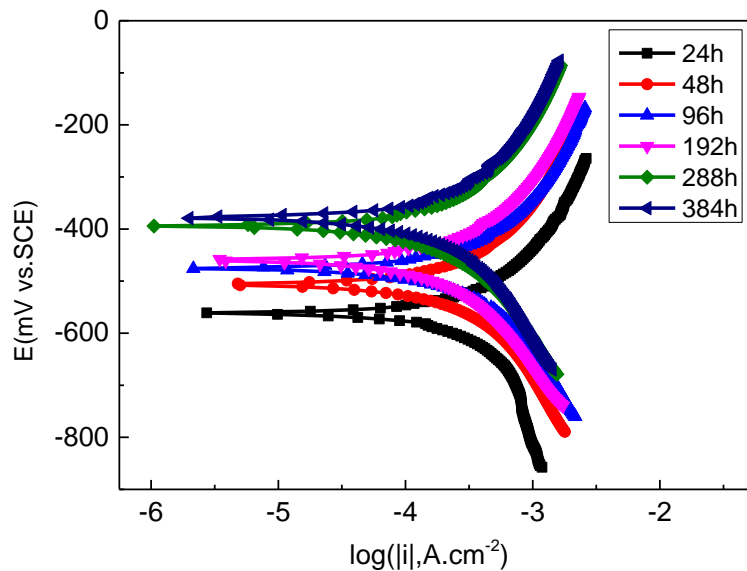


Figure 8. Potentiodynamic polarization curves of the test steel under H₂S/CO₂ environment at 75°C after different immersion time

The electrochemical fitting parameters are applied by Tafel extrapolation, the corrosion kinetics parameters such as anodic Tafel slope (ba) and cathodic Tafel slope (bc), corrosion current density (I_{corr}), corrosion potential (E_{corr}), the fitting data are given in Table 2. According to research found that the

smaller corrosion current density, the lower corrosion rate and the less likely it is to corrode. The self-corrosion potential of studied steel is moving into the positive direction with immersion time, implying good corrosion resistance [32]. The corrosion current density changes from 0.5642 mA to 0.1185 mA, decreasing about 0.4457 mA. the self-corrosion potential changes from -562 mV to -379 mV, increasing about 183 mV. Based on the above analysis, the corrosion resistance increases with the prolonging of immersion time. the obtained results of polarization curves measurements are consistent with immersion tests.

Table 2. Electrochemical parameters of polarization curves of the test steel under H₂S/CO₂ environment at 75°C after different immersion time

Immersion time (h)	b _a (mV/dec)	b _c (mV/dec)	I _{corr} (mA/cm ²)	E _{corr} (mV)
24	321	581	0.5642	-562
48	236	273	0.2681	-507
96	196	223	0.2345	-476
192	179	244	0.1774	-460
288	178	197	0.1273	-395
384	170	193	0.1185	-379

4. CONCLUSIONS

The corrosion characteristics of ferrite-pearlite steel immersed in H₂S/CO₂ environment are studied. The corrosion properties are analyzed on the basis of microstructure, morphology, cross sectional morphology, corrosion phases, corrosion kinetics and potentiodynamic polarization curve. The corrosion behavior includes three phases according to the test results, it goes down quickly in the early stages, then flattens out, finally the corrosion rate is almost constant. The corrosion products change as follows with time: mackinawite-troilite-pyrrhotite, H₂S plays an important role, and mackinawite crystals control the whole corrosion process. The films have two layers including inner and outer layers, the double-layer compact corrosion film can act as an effective barrier against diffusion.

ACKNOWLEDGEMENTS

This work was supported by the China Postdoctoral Science Foundation (No.2018M631761), the Fundamental Research Funds for the Central Universities (No. N182303030), the Higher Educational Science and Technology Program of Hebei Province (No. QN2019317) and the Natural Science Foundation of China (No.61903072).

References

1. W. Wu, Y. Li, G. X. Cheng, H. Zhang, J. Kang, *Eng. Fail Anal.*, 98 (2019) 156.
2. H. W. Wang, H. Y. Wang, X. H. Gao, C. Yu, *Int. J. Electrochem. Sci.*, 14 (2019) 10907.
3. B. H. Xu, B. Yuan, Y. Q. Wang, L. Zhu, *Constr. Build. Mater.*, 188 (2018) 161.

4. M. Askari, M. Aliofkhazraei, S. Ghaffari, A. Hajizadeh, *J. Nat. Gas Sci. Eng.*, 58 (2018) 92.
5. J. W. Zhao, Z. Y. Jiang, C. S. Lee, *Corros. Sci.*, 82 (2014) 380.
6. P. F. Sui, J. B. Sun, Y. Hua, H. F. Liu, *Int. J. Greenh. Gas Con.*, 73 (2018) 60.
7. Z. Y. Cui, Z. Y. Liu, L. W. Wang, H. C. Ma, C. W. Du, X. G. Li, X. Wang, *J. Mater. Eng. Perform.*, 24 (2015) 4400.
8. W. F. Li, Y. J. Zhou, Y. Xue, *J. Iron Steel Res. Int.*, 19 (2012) 59.
9. W. He, O. Ø. Knudsen, S. Diplas, *Corros. Sci.*, 51 (2009) 2811.
10. Z. Aslam, R. A. Shawabkeh, I. A. Hussein, A. Al-baghli, M. Eic, *Appl. Surf. Sci.*, 327 (2015) 107.
11. H. S. Song, M. G. Park, E. Croiset, Z. W. Chen, S. C. Nam, H. J. Ryu, K. B. Yi, *Appl. Surf. Sci.*, 280 (2013,) 360.
12. G. A. Zhang, Y. Zeng, X. P. Guo, *Corros. Sci.*, 65 (2012) 37.
13. Z. F. Yin, W. Z. Zhao, Z. Q. Bai, Y. R. Feng, W. J. Zhou, *Electrochim. Acta*, 53 (2008) 3690.
14. X. H. Zhao, Y. Han, Z. Q. Bai, B. Wei, *Electrochim. Acta*, 56 (2011) 7725.
15. C. Yu, P. Wang, X. H. Gao, *Int. J. Electrochem. Sci.*, 10 (2015) 6820.
16. Y. S. Choi, S. Nesic, S. Ling, *Electrochim Acta*, 56 (2011) 1752.
17. K. Masamura, S. Hashizume, *Corros.*, 43 (1987) 359.
18. C. Yu, X. H. Gao, H. W. Wang, *Mater. Lett.*, 209 (2017) 459.
19. L. Wei, X. L. Pang, K. W. Gao, *Corros. Sci.*, 103 (2016) 132.
20. C. Sun, Y. Wang, J. B. Sun, X. Q. Lin, X. D. Li, H. F. Liu, X. K. Cheng, *J. Supercrit Fluid*, 116 (2016) 70.
21. J. B. Sun, C. Sun, G. A. Zhang, X. D. Li, W. M. Zhao, T. Jiang, H. F. Liu, X. K. Cheng, Y. Wang, *Corros. Sci.*, 107 (2016) 31.
22. X. H. Zhao, Y. Han, Z. Q. Bai, B. Wei, *Electrochim. Acta*, 56 (2011) 7725.
23. L. D. Wang, H. B. Wu, Y. T. Liu, H. W. Zhang, L. F. Liu, D. Tang, *Mater. Sci., Technol.*, 21 (2013) 8.
24. H. B. Wu, L. F. Liu, L. D. Wang, Y. T. Liu, *J. Iron Steel Res. Int.*, 21 (2014) 76.
25. Q. Y. Wang, X. Z. Wang, H. Luo, J. L. Luo, *Surf. Coat Tech.*, 291 (2016) 250.
26. Z. G. Liu, X. H. Gao, L. X. Du, J. P. Li, Y. Kung, B. Wu, *J. Mater. Eng. Perform.*, 26 (2017) 1010.
27. F. X. Shi, L. Zhang, J. W. Yang, M. X. Lu, J. G. Ding, H. Li, *Corros. Sci.*, 102 (2016) 103.
28. M. Liu, J. Q. Wang, W. Ke, E. H. Han, *J. Mater. Sci. Technol.*, 30 (2014) 504.
29. D. W. Shoesmith, P. Taylor, M. G. Bailey, D. G. Owen, *J. Electrochem. Soc.*, 127 (1980) 1007.
30. P. P. Bai, S. Q. Zheng, C. F. Chen, *Mater. Chem. Phys.*, 159 (2015) 295.
31. W. F. Li, Y. J. Zhou, Y. Xue, *J. Wuhan. Univ. Technol. Mater. Sci.*, 28 (2015) 1038.
32. D. J. Kong, W. Guo, *J. Cent. South Univ.*, 22 (2015) 3722.